

Depinning of domain walls with an internal degree of freedom

V. Lecomte,¹ S. E. Barnes,^{1,2} J.-P. Eckmann,³ and T. Giamarchi¹

¹*DPMC-MaNEP, University of Geneva, 24 quai Ernest-Ansermet, 1211 Geneva 4, Switzerland*

²*Physics Department, University of Miami, Coral Gables, FL 33124, USA*

³*Department of Theoretical Physics and Section de Mathématiques, University of Geneva, 24 quai Ernest-Ansermet, 1211 Geneva 4, Switzerland*

Taking into account the coupling between the position of the wall and an internal degree of freedom, namely its phase φ , we examine, in the rigid wall approximation, the dynamics of a magnetic domain wall subject to a weak pinning potential. We determine the corresponding force-velocity characteristics, which display several unusual features when compared to standard depinning laws. At zero temperature, there exists a bistable regime for low forces, with a logarithmic behavior close to the transition. For weak pinning, there occurs a succession of bistable transitions corresponding to different topological modes of the phase evolution. At finite temperature, the force-velocity characteristics become non-monotonous. We compare our results to recent experiments on permalloy nanowires.

PACS numbers: 05.10.Gg, 05.45.-a, 64.60.Ht, 75.70.-i

Many physical systems comprise different phases which coexist and are separated by an interface. Examples range from magnetic [1, 2, 3, 4] or ferroelectric [5, 6] domain walls (DWs), to growth surfaces [7, 8] or contact lines [9]. Common to this large variety of phenomena is a macroscopic description within which the interface properties are well described by a competition between the elasticity, which tends to minimize the interface length, and the local potential, whose valleys and hills deform the interface so as to minimize its total energy.

Such interfaces are described by the theory of disordered elastic systems [10, 11], which explains well their static (e.g., roughness at equilibrium, correlation functions) as well as dynamical features (transient regime, response to a field). The existence of a threshold force f_c below which the system is pinned is a crucial feature of the zero-temperature motion of such an interface. When $f \gtrsim f_c$ the velocity $v \sim (f - f_c)^\beta$ is characterized by a depinning exponent β , while at finite temperature $v \sim T^\psi$ at $f = f_c$ defines the thermal exponent ψ . Some predicted exponents are in very good agreement with measurements, e.g., in magnetic [1] or ferroelectric [6] films, while discrepancies remain for contact lines [9] or for magnetic wires [12], and one can ask what are the missing ingredients in the description. In particular, it is usual in the macroscopic description to specify only the position of the interface, discarding, a priori, as irrelevant internal structures. Here we investigate how this position couples to an internal degrees of freedom, and how this coupling is manifested in experiment.

In magnetic systems, the DW position is generically coupled to an internal degree of freedom (a spin phase φ [35]). An interesting case is the motion of a 180° DW in a narrow ferromagnetic thin film, which has been the subject of intense experimental study because of its importance for spintronics [12, 13, 14, 15]. It is known [16], in the absence of pinning, that $v(f)$ increases up to a

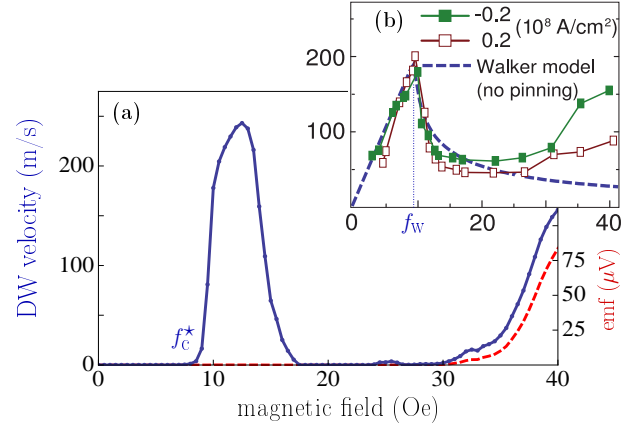


FIG. 1: (color online) (a) Finite temperature, zero current ($j_s = 0$) force-velocity curves (blue, solid) and emf $\frac{\hbar}{e} \langle \dot{\varphi} \rangle$ (red, dashed) for a DW with pinning. Parameters correspond to experiments shown in (b). Adapted from Ref. [13], the data (squares) are for small but opposite currents. In the absence of pinning (Walker model, dashed blue line) there is no second rapid increase in v manifest in the data.

characteristic ‘Walker’ force f_w above which the velocity actually *decreases* up to values $f \gg f_w$ (Fig.1). In contrast standard interface theory [10] takes pinning into account but not the phase, yielding a monotonous $v(f)$. An approach combining these two ingredients is missing.

In this Letter, we develop such an approach and show there are dramatic changes as compared with both the Walker picture and standard interface theory. Specifically, the DW is pinned up to a force f_c^* above which the depinning law is bistable and logarithmic. Even more strikingly, as f is increased further, the velocity falls back to zero until a second depinning transition occurs (Fig.1). This is followed by a cascade of such transitions until finally $v(f)$ becomes monotonous. Upon adding the effects of a finite temperature, this offers a natural explanation of the two peaks of $v(f)$ observed in experiments [13].

We consider an uniaxially anisotropic ferromagnetic medium with position-dependent magnetization of direction $\mathbf{\Omega} = (\sin\theta \cos\varphi, \sin\theta \sin\varphi, \cos\theta)$ with easy z -axis and hard y -axis with respective anisotropy constants K and K_\perp . With spin stiffness J , the energy $E[\mathbf{\Omega}]$ is [17]

$$E = \frac{1}{2} \int d^3x \left\{ J \left[(\nabla\theta)^2 + \sin^2\theta (\nabla\varphi)^2 \right] + K \sin^2\theta + K_\perp \sin^2\theta \cos^2\varphi \right\}$$

The corresponding Landau-Lifshitz dynamics reads

$$(\partial_t + v_s \nabla) \mathbf{\Omega} = \mathbf{\Omega} \times (H + \tilde{\eta}) - \mathbf{\Omega} \times (\alpha \partial_t + \beta_s v_s \nabla) \mathbf{\Omega} \quad (1)$$

Here, $H = -\delta E/\delta \mathbf{\Omega} + f_{\text{ext}}$ and f_{ext} is the external field and α is the Gilbert damping, which accounts for dissipation. The velocity v_s [36] is proportional to the spin-polarized current density j_s and β_s is the current-induced relaxation. The white noise $\tilde{\eta}$ accounts for thermal fluctuations for temperature T [37]. Below the Walker field $f_w = \frac{1}{2}\alpha K_\perp$, and for $T = 0$, there exists a solution to (1) for constant f_{ext} [16]: $\theta(x, t) = 2 \arctan \exp[(x/\lambda - v_w t)/\xi]$ with $\xi = [1 + (K_\perp/K) \sin\varphi]^{-1/2}$ and constant $\varphi(x, t) = \frac{1}{2} \arcsin f_{\text{ext}}/f_w$. This represents a Néel DW of width $\lambda = \sqrt{J/K}$ and velocity $v_w = \xi f_{\text{ext}}/f_w$ [38].

In more general situations, this domain wall solution with $v_w t$ replaced by the actual position $r(t)$ and with this and $\varphi(t)$ considered as parameters is used as an ansatz. In the rigid wall approximation (constant ξ), one obtains the effective equations [16, 18, 19, 20, 21, 22]

$$\alpha \partial_t r - \partial_t \varphi - \beta_s v_s = f_{\text{ext}}(r) + \eta_1 \quad (2)$$

$$\alpha \partial_t \varphi + \partial_t r - v_s = -\frac{1}{2} K_\perp \sin 2\varphi + \eta_2 \quad (3)$$

($\lambda = 1$ by choice of length units [39].) We split the external field $f_{\text{ext}}(r) = f - V'(r)$ into a constant ‘depinning’ (or ‘tilt’) force f and a ‘pinning’ force $-V'(r)$ deriving from a potential V . The effective thermal noise is now [22] $\langle \eta_i(t) \eta_j(t') \rangle = 2(\hbar N)^{-1} \alpha k_B T \delta(t' - t) \delta_{ij}$ where $N = 2\lambda A/a^3$ is the number of spins in the DW, of section A . For constant fields $f > f_w$, this ansatz reproduces very accurately [16] the numerical solution of the bulk equation (1). We checked that this result also extends to the case of a non-uniform potential landscape [23].

Having simplified (1) to (2-3), we further restrict our study to the case $j_s = 0$: current effects will be considered elsewhere [23]. The potential $V(r)$ should reflect the pinning effects of impurities or local variations in the couplings. A proper treatment of a realistic disordered $V(r)$ is a delicate task and in order to gain insights into the full problem we take a periodic $V(r) = \frac{1}{\kappa} \sin \kappa r$ [40].

We first consider the zero-temperature motion. Before embarking into a thorough analysis of (2-3), let us gain some insights from simple considerations. At $f = 0$, the wall is pinned in one of the minima of $V(r) = \frac{1}{\kappa} \sin \kappa r$. There exists a characteristic force f_c beyond which local minima of the tilted potential $\frac{1}{\kappa} \sin \kappa r - fr$ disappear

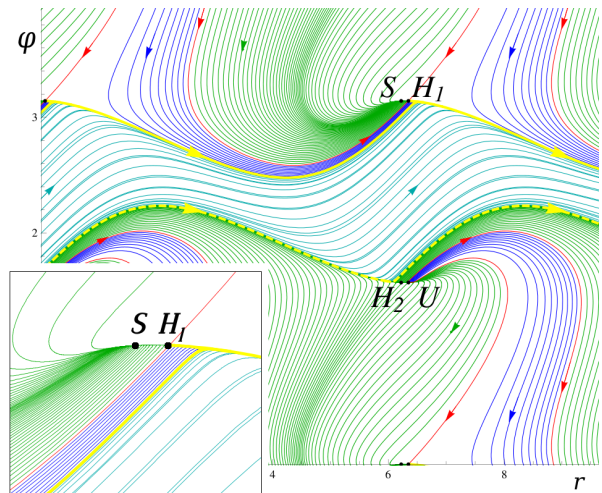


FIG. 2: (color online) Phase space trajectories (r, φ) for f in the bistable regime ($f_c^* < f < f_c$). $S, U, H_{1,2}$ are the fixed points. Blue and turquoise trajectories converge to the attracting limit cycle (yellow). Those in green end at the stable fixed point S . Separatrices (red) mark the boundaries between the corresponding regions. The repulsive limit cycle (dashed yellow) is also a separatrix.

(here $f_c = 1$). Ignoring the variable φ , the wall would start to move at $f = f_c$ and acquire a finite mean velocity at long times for $f > f_c$, because of damping. But since r is coupled to φ , the wall may store enough kinetic energy in φ to cross barriers for forces less than f_c , hence shifting the depinning transition to some $f_c^* < f_c$. For f between these values, the system is bistable: depending on the initial condition, the wall is either pinned in a minimum or slides down in the tilted landscape while φ oscillates around its own minimum. Moreover, the periodicity of φ can induce an unexpected effect: increasing f makes φ cross its own barrier and fall into its next minimum, but this has a cost: dissipation increases and φ cannot give back enough kinetic energy to r . This intuitive picture explains the valley appearing in $v(f)$ (Fig.1) until the depinning force injects enough energy to reach another regime where both φ and r increase in time.

The analysis of (2-3) can be put on a firm basis by considering the phase space of (r, φ) , which is a torus of period $2\pi/\kappa$ in r and π in φ . We determine the nature of the possible trajectories. These cannot cross in phase space, but can meet at the fixed points (steady solutions of (2-3)). Trajectories approaching a stable fixed point have zero mean velocity $v \equiv \langle \partial_t r \rangle$, unlike those moving along a limit cycle. In the latter case the particle covers one spatial period $2\pi/\kappa$ over a period of time τ , so that the average velocity is given by $v = 2\pi/(\kappa\tau)$. We will thus determine $v(f)$ through τ .

We remark that (2-3) has no fixed points for $f > f_c$, which means that the DW moves with non-zero velocity. For $f < f_c$, there are four fixed points of coordinates (Fig.2): $H_1 = (r_0, 0)$ and $H_2 = (-r_0, \pi/2)$, which are hyperbolic (i.e., with one unstable and one stable direc-

tion), $S = (-r_0, 0)$, totally stable, and $U = (r_0, \pi/2)$, totally unstable; here $r_0 = \arccos f > 0$. The decomposition of the phase space into different dynamical regimes depends on the value of K_\perp , which determines how much φ can depart from 0 (see [23] for full details):

(i) *Case of high K_\perp* : all trajectories end at S , i.e., there are no limit cycles ($v = 0$). This regime persists until $f = f_c$, at which point the pairs (H_1, S) , (H_2, U) merge and give rise to a saddle-node bifurcation [24]. For small $\delta f \equiv f - f_c > 0$, we have $\alpha \partial_t r \simeq \delta f + \frac{1}{2} r^2$ in the region $r \simeq 0$ where the trajectory spends most of its time, whence $r(t) = \sqrt{2\delta f} \tan[t\sqrt{\delta f/2}]$ and one recovers the standard depinning law with exponent $\beta = \frac{1}{2}$ (Fig.3.b).

(ii) *Case of intermediate K_\perp* : there is in addition a second critical force $f_c^* < f_c$ (Fig.3.b). For $f < f_c^*$ all trajectories end at S . For $f_c^* < f < f_c$ one has bistability: depending on the initial condition (Fig.2), trajectories either end at S ($v = 0$ branch in $v(f)$) or move along an attracting limit cycle ($v > 0$ branch). In that case, the bifurcation is homoclinic [24] and f_c^* is the value of the force for which the trajectory starting in an unstable direction of H_1 returns exactly to H_1 (see Fig.3.a). The value of f_c^* depends on global aspects, in contrast to the case (i). The depinning law of the $v > 0$ branch is evaluated as follows (see [23]): the trajectory spends most of its time close to the hyperbolic point H_1 , of positive Lyapunov exponent Λ so that $r(t) \simeq (f - f_c^*)e^{\Lambda t}$. The period τ thus verifies $2\pi/\kappa \sim (f - f_c^*)e^{\Lambda\tau}$ and up to factors:

$$v \propto |\log(f - f_c^*)|^{-1} \quad (4)$$

(iii) *Case of smaller K_\perp* : here, the particularly novel features appear, with a depinning law $v(f)$ characterized by a succession of bistable regimes (Fig.4.b) separated by regions of zero velocity. An interesting mechanism emerges: in general, the first bistable regime is characterized by cycling trajectories with r advancing and φ oscillating within a bounded interval, but with increasing force, φ will eventually rotate by a whole period of π , and fall into S . At this point there is a collision between the stable and unstable limit cycles (of Fig.2), and the original type of limit cycle disappears for larger forces resulting in an intermediate $v = 0$ valley. Increasing f even more, the phase space reorganizes until there appear trajectories with both r and φ increasing with each period of the limit cycle (Fig.4.b). Each bistable regime is governed by the same bifurcation as in case (ii), but is now also characterized by the number of windings of r and φ during τ . This striking phenomenon, a *topological transition*, arises from the periodicity of the phase and cannot appear for instance in situation where r couples to an unbounded variable (e.g., the momentum of a massive particle in a periodic potential). But topological transitions can potentially be found in other systems, e.g., for viscously coupled particles in a periodic potential [25], described by equations similar to (2-3), although $v(f)$ is

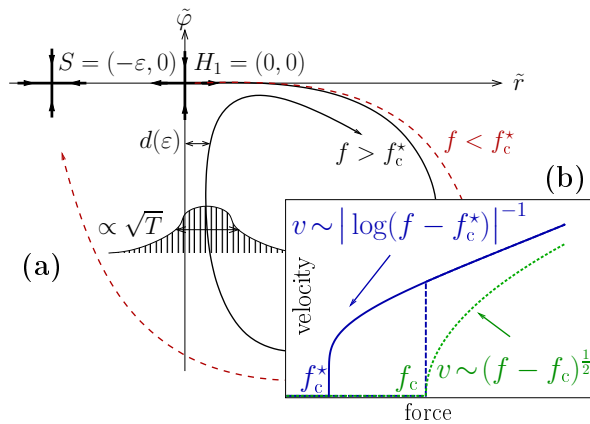


FIG. 3: (color online) (a) Sketch of the phase space for the coordinates $(\tilde{r}, \tilde{\varphi})$, and homoclinic bifurcation. For $f < f_c^*$ (red, dashed), trajectories all end at S . For $f > f_c^*$ (black, solid), the line starting from the unstable direction of H_1 converges to the limit cycle. At $T > 0$, the random evolution has Gaussian probability distribution of variance $\propto \sqrt{T}$. (b) The two types of depinning laws at $T = 0$. For large K_\perp (green, dotted) depinning occurs with $\beta = \frac{1}{2}$. For intermediate K_\perp (blue, solid) there is a bistable regime of force ($f_c^* < f < f_c$) with a zero-velocity branch and a non-zero one in $1/\log$.

found to be monotonous for the conditions of [25].

We finally address the finite temperature dynamics in the regime $f_c^* < f < f_c$, of particular interest since thermal fluctuations cause the system to forget its initial condition, and thus destroy the bistability. Taking normal coordinates close to H_1 , (Fig.3) the evolution follows $\partial_t \tilde{r} = \varepsilon \tilde{r} + \tilde{r}^2 + \eta$, $\partial_t \tilde{\varphi} = -\tilde{\varphi}$ (with $\varepsilon \propto f_c - f > 0$). Starting from H_1 towards the limit cycle and evolving with the noisy dynamics, the trajectory comes back to H_1 with a Gaussian distribution of width $\propto \sqrt{T}$ at distance $d(\varepsilon) \propto \varepsilon - \varepsilon_c^*$ from the separatrix (Fig.3.a). The mean escape time is determined by a competition between the large Arrhenius time to escape from the local potential trap $\tilde{V}(\tilde{r}) = -\varepsilon \tilde{r}^2/2 - \tilde{r}^3/3$ and the small probability $\sim \exp(-d(\varepsilon)^2/T)$ of falling into it [23]:

$$\tau_{\text{escape}} \sim \exp\left(\frac{\varepsilon^3}{3T} - A \frac{(\varepsilon - \varepsilon_c^*)^2}{T}\right) \quad (5)$$

Thus for $T > 0$, the bistability curve is transformed in the following manner: the curves $v(f, T)$ all cross at some new characteristic force f_c^{**} (where the polynomial in ε in (5) has a zero)[41]. For $f < f_c^{**}$, the depinning is dominated by the escape from the trap while for $f > f_c^{**}$, $v(f, T)$ approaches the positive branch of the $T = 0$ law (Fig.4.a). In the limit $T \rightarrow 0^+$, $v(f)$ is monostable and discontinuous in f_c^{**} , in contrast with the $T = 0$ case. Note that Vollmer and Risken [26, 27] have studied the dynamics of a massive particle in a periodic potential, for $T > 0$, with results related to those of Fig.4.a, but with an approach limited to that particular problem and only valid in the small α regime. In contrast, our approach not only displays a non-monotonous $v(f)$ but also allows

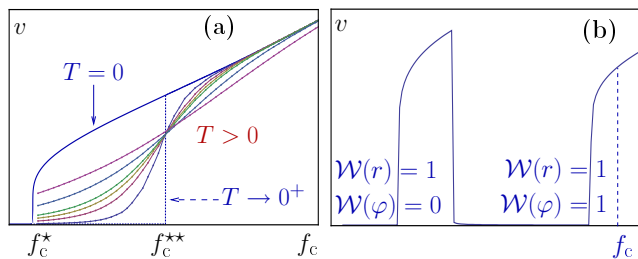


FIG. 4: (color online) **(a)** For any finite T there exists a critical field f_c^{**} such that for $f < f_c^{**}$ the albeit small probability of falling into the trap S exceeds that of escape and the velocity is small while the inverse is true for $f > f_c^{**}$. The curves approach the vertical line as $T \rightarrow 0$ and all curves cross at $f = f_c^{**}$ to first order in T . **(b)** For smaller K_{\perp} (and $T = 0$), successive bistable transitions occur, indexed by the winding numbers $\mathcal{W}(r)$ and $\mathcal{W}(\varphi)$ of r and φ on one period.

for a general discussion of what happens in the vicinity of a homoclinic bifurcation for any α , in the perspective of stochastic differential equations, and is more in the spirit of Freidlin and Wentzell [28, 29].

Despite the oversimplified features of our model, it offers a possible resolution of an experimental mystery [13]. In the absence of pinning ($V = 0$), and corresponding to the simple Walker breakdown picture it is possible to reproduce the first peak of $v(f)$ for parameters similar to those of [13] ($\alpha = 1.32 \times 10^{-2}$, $K_{\perp} = 1500$ Oe, corresponding to $f_w = 9.9$ Oe, $v_w = 200$ m/s), but $v(f)$ has only a peak without the valley seen in the experimental data (Fig.1.b). In contrast, due to the existence of a *topological transition*, for finite V the velocity v falls towards zero following a first peak and only rises again for larger values the force f . Indeed, simulations [42] of (2-3) reproduce the ‘valley’ observed in $v(f)$ for similar parameters ($\alpha = 5 \times 10^{-2}$, $K_{\perp} = 1200$ Oe, $V_0 = 50$ Oe, $\kappa = 5.15/\lambda$). We predict in particular the following watermark for the topological transition: the second peak should coincide with the appearance of non-zero $\langle \dot{\varphi} \rangle$, measurable through the emf [30] $\frac{\hbar}{e} \langle \dot{\varphi} \rangle$ (Fig.1.a) while in the Walker picture $\langle \dot{\varphi} \rangle > 0$ immediately for $f > f_w$.

To summarize, we have shown how the coupling between the phase and the position of a rigid wall in 1D dramatically affects the depinning law, which displays bistabilities and an unusual scaling $v \propto 1/|\log(f - f_c^*)|$. Due to the periodicity of the phase, there are conditions for which different bistable regimes follow one another with increasing f , yielding for $T > 0$ a *non-monotonous* $v(f)$, which might well explain features of recent measurements [13]. It would be valuable to consider the current-driven case ($v_s \neq 0$), of interest in the context of spintronics. Moreover, the solitonic ansatz can also describe interfaces with non-zero dimension, where the interplay between the phase and the elastic deformations potentially affects the creep motion and the depinning.

This work was supported in part by the Swiss NSF under MaNEP and Division II.

- [1] S. Lemerle *et al.*, Phys. Rev. Lett. **80**, 849 (1998).
- [2] M. Bauer *et al.*, Phys. Rev. Lett. **94**, 207211 (2005).
- [3] M. Yamanouchi *et al.*, Phys. Rev. Lett. **96**, 096601 (2006).
- [4] P. J. Metaxas *et al.*, Phys. Rev. Lett. **99**, 217208 (2007).
- [5] P. Paruch, T. Giamarchi, and J.-M. Triscone, Phys. Rev. Lett. **94**, 197601 (2005).
- [6] P. Paruch and J.-M. Triscone, Appl. Phys. Lett. **88**, 162907 (2006).
- [7] A.-L. Barabasi and H. E. Stanley, *Fractal Concepts in Surface Growth* (Cambridge University Press, 1995).
- [8] J. Krim and G. Palasantzas, Int. J. Mod. Phys. B **9**, 599 (1995).
- [9] S. Moulinet *et al.*, Phys. Rev. E **69**, 035103 (2004).
- [10] M. Kardar, Phys. Rep. **301**, 85 (1998).
- [11] T. Giamarchi and P. Le Doussal, *Statics and dynamics of disordered elastic systems* (World Scientific, Singapore, 1998), p. 321, cond-mat/9705096.
- [12] M. Yamanouchi *et al.*, Science **317**, 1726 (2007).
- [13] S. S. P. Parkin, M. Hayashi, and L. Thomas, Science **320**, 190 (2008).
- [14] A. Yamaguchi *et al.*, Phys. Rev. Lett. **92**, 077205 (2004).
- [15] L. Thomas *et al.*, Nature **443**, 197 (2006).
- [16] N. L. Schryer and L. R. Walker, J. Applied Phys. **45**, 5406 (1974).
- [17] L. D. Landau, E. M. Lifshitz, and L. Pitaevskii, *Electrodynamics of Continuous Media* (Pergamon Press, Oxford, 1960).
- [18] A. P. Malozemoff and J. C. Slonczewski, *Magnetic domain walls in bubble materials* (Academic Press, New York, 1979).
- [19] J. C. Slonczewski, J. Mag. Mag. Mat. **159**, L1 (1996).
- [20] G. Tatara and H. Kohno, Phys. Rev. Lett. **92**, 086601 (2004).
- [21] S. E. Barnes and S. Maekawa, Phys. Rev. Lett. **95**, 107204 (2005).
- [22] R. A. Duine, A. S. Núñez, and A. H. MacDonald, Phys. Rev. Lett. **98**, 056605 (2007).
- [23] V. Lecomte, S. E. Barnes, J.-P. Eckmann, T. Giamarchi, in preparation.
- [24] P. H. J. Guckenheimer, *Nonlinear Oscillations, Dynamical Systems, and Bifurcations of Vector Fields* (Springer-Verlag, New York, 2002).
- [25] P. Le Doussal, M. C. Marchetti, and K. J. Wiese, Phys. Rev. B **78**, 224201 (2008).
- [26] H. D. Vollmer and H. Risken, Z. Phys. B **37**, 343 (1980).
- [27] H. Risken, *The Fokker-Planck equation* (Springer-Verlag, Berlin, 1996).
- [28] H. Freidlin and D. Wentzell, *Random perturbations of dynamical systems* (Springer-Verlag, Berlin, 1984).
- [29] J.-P. Eckmann, L. Thomas, and P. Wittwer, J. Phys. A **14**, 3153 (1981).
- [30] S. E. Barnes and S. Maekawa, Phys. Rev. Lett. **98**, 246601 (2007).
- [31] W. F. Brown, Phys. Rev. **130**, 1677 (1963).
- [32] G. Tatara, H. Kohno, and J. Shibata, J. Phys. Soc. Jpn. **77**, 031003 (2008).
- [33] B. Derrida, J. Stat. Phys. **31**, 433 (1982).
- [34] P. Le Doussal and V. M. Vinokur, Physica C **254**, 63 (1995).
- [35] Although this coupling is well known in the magnetic

DW community [18], it has to our knowledge always been discarded in interface physics.

- [36] $v_s = Pj_s/(e\rho_s)$ with P the current polarization, e the carrier charge and ρ_s the spin density.
- [37] It has zero mean and variance [31]: $\langle \tilde{\eta}_i(\mathbf{x}, t)\tilde{\eta}_j(\mathbf{x}', t') \rangle = 2\hbar^{-1}\alpha k_B T \delta(\mathbf{x}' - \mathbf{x}) \delta(t' - t) \delta_{ij}$.
- [38] Bloch DWs are treated similarly [32].
- [39] We also translated $\varphi \rightarrow \varphi + \frac{\pi}{2}$ for convenience.
- [40] For an overdamped particle in an arbitrary potential [33, 34], taking $V(r)$ random yields $r(t) \sim t^\gamma$ and $v(f)$ is

not finite in general, while taking $V(r)$ periodic leads to standard depinning with $\beta = \frac{1}{2}$ and $\psi = \frac{1}{3}$.

- [41] This is at variance with the thermal rounding of the $v \sim (f - f_c)^\beta$ law, which develops no crossings for $T > 0$.
- [42] In simulations we discretize (2-3) in time ($> 10^6$ steps with $dt = 5 \times 10^{-3}$) and average over 2048 realizations. In both cases, the DW width was taken to $\lambda = 15$ nm [13] and the temperature to $T = 300$ K.